

# A Chandra HETGS observation of the Narrow-line Seyfert 1 galaxy Ark 564

Chiho Matsumoto and Karen M. Leighly

*Department of Physics and Astronomy, The University of Oklahoma, 440 W. Brooks St.,  
Norman, OK 73019*

chiho,leightly@nhn.ou.edu

and

Herman L. Marshall

*MIT Center for Space Research, 77 Massachusetts Ave., Cambridge, MA 02139*

## ABSTRACT

We present results from a 50 ks observation of the narrow-line Seyfert 1 galaxy Ark 564 with the *Chandra* HETGS. The spectra above 2 keV are modeled by a power-law with a photon-index of  $2.56 \pm 0.06$ . We confirm the presence of the soft excess below about 1.5 keV. If we fit the excess with blackbody model, the best-fit temperature is 0.124 keV. Ark 564 has been reported to show a peculiar emission line-like feature at 1 keV in various observations using lower resolution detectors, and the *Chandra* grating spectroscopy rules out an origin of blends of several narrow emission lines. We detect an edge-like feature at 0.712 keV in the source rest frame. The preferred interpretation of this feature is combination of the O VII K-edge and a number of L-absorption lines from slightly ionized iron, which suggests a warm absorber with ionization parameter  $\xi \sim 1$  and  $N_{\text{H}} \sim 10^{21} \text{ cm}^{-2}$ . These properties are roughly consistent with those of the UV absorber. We also detect narrow absorption lines of O VII, O VIII, Ne IX, Ne X, and Mg XI at the systemic velocity. From these lines, a second warm absorber having  $\log \xi \sim 2$  and  $N_{\text{H}} \sim 10^{21} \text{ cm}^{-2}$  is required.

*Subject headings:* galaxies: Seyfert, galaxies: X-ray, individual: Ark 564

## 1. Introduction

Narrow-line Seyfert 1 galaxies (NLS1s) belong to a ubiquitous class of X-ray luminous AGNs whose extreme spectral and variability properties have been the subject of intensive

study by virtually every X-ray satellite during the past decade. Defined by their optical emission-line properties (FWHM  $H\beta < 2000 \text{ km s}^{-1}$  and  $[O III] \lambda 5007/H\beta < 3$ ) NLS1s are different from type 2 Seyfert galaxies, which generally have  $[O III]/H\beta > 3$  (Osterbrock & Pogge 1985; Goodrich 1989). NLS1s usually have strong permitted lines of Fe II, resembling the well-known prototype of their class, I Zw 1.

The extreme X-ray properties of Narrow-line Seyfert 1 galaxies are now well established. They frequently show a strong soft excess component, their hard X-ray spectrum tends to be steeper than in similar broad-line Seyfert 1 galaxies, and they show enhanced X-ray variability (e.g., Leighly 1999a,b and references therein). The most promising explanation for this behavior is that NLS1s have a higher mass accretion rate with respect to the Eddington value than ordinary Seyfert galaxies with broad optical lines (Laor 2000). This result is potentially very important: since AGN are believed in general to be powered by accretion, study of objects with the highest accretion rate may help us understand AGN accretion in general.

Ark 564 ( $z=0.02468\pm 0.00007$ ; Huchra, Vogeley, & Geller 1999) is an interesting object from the point of view that shows a peculiar emission line-like feature near 1 keV in low resolution spectra. This emission line-like feature has been reported from various observations performed by *ROSAT*, *ASCA* and *BeppoSAX* (Brandt et al. 1994; Leighly 1999b; Turner, George, & Netzer 1999; Comastri et al. 2001). Turner et al. (1999) modeled the feature with a strong (equivalent width:  $EW\sim 70 \text{ eV}$ ) and relatively broad ( $\sigma=0.16 \text{ keV}$ ) line at  $0.99^{+0.02}_{-0.04} \text{ keV}$ , assuming that spectral components are Galactic absorption, a power-law and a Gaussian line in the energy band of 0.6–5.0 and 7.5–10 keV. Using the same data and the different continuum model (Galactic absorbed a power-law plus a black body), Leighly (1999b) obtained weaker ( $EW= 30 \text{ eV}$ ) line at  $1.033^{+0.024}_{-0.031} \text{ keV}$  with  $\sigma$  of 0.1 eV. Comastri et al. (2001) also reported that the model dependent EW is as low as 20–50 eV with the same model as Leighly’s from independent analyses. In the *BeppoSAX* observation, a line-like feature around 1 keV is clearly visible (Comastri et al. 2001). Still the origin of this feature was far from being unambiguously identified.

In order to identify this feature, we carried out an observation with the *Chandra* High Energy Transmission Grating Spectrometer (HETGS). Observed with higher energy resolution, some possible origins for this feature, such as blends of narrow emission lines, can be investigated. If we can identify this feature, it may enable us to investigate the physical conditions such as ionization state of the surrounding matter of the AGN. Ark 564 is one of the brightest narrow-line Seyfert 1 galaxies in the hard X-ray band and the 2–10 keV flux is a few times  $10^{-11} \text{ erg cm}^{-2} \text{ s}^{-1}$ , so a grating observation using *Chandra* is clearly feasible.

In this paper, we will report the fine spectroscopy of Ark 564. Section 2 describes the

details of the observations and data reduction. In §3, the analysis of power spectral density is performed. §4 contains the spectral analysis. We detected many absorption lines, but no prominent narrow emission line around 1 keV is detected. In §5, we discuss the inferred photoionization model and the location of warm absorber. We also find that the 1 keV emission line feature appears to be an artifact of the warm absorber. Finally, we summarize the results in §6.

## 2. Observations

We carried out an observation of Ark 564 with the *Chandra* HETGS on 2000 June 17 06:50–21:05. The detector was the Advanced CCD Imaging Spectrometer (ACIS). Our observation was 50 ks in duration and continuous. We analyzed the most recent standard processed level 2 data (revision 3) using the CIAO version 2.2.0, CALDB version 2.9, and HEASoft version 5.1.

The peak of the zeroth order image is located at R.A.= 22<sup>h</sup>42<sup>m</sup>39.33<sup>s</sup> and Decl.= 29°43′31.6 (equinox 2000.0) in good agreement with the optical position of R.A.= 22<sup>h</sup>42<sup>m</sup>39.345<sup>s</sup>, Decl.= 29°43′31.31 (Clements 1981) with the *Chandra* spatial resolution (0.49 arcsec/pixel).

Since the HETGS response matrices are subject to the extension of the source, we checked whether or not the source is point-like. At first, we looked at the zeroth order image. We found the image is circular in shape, thus asymmetry possibly associated with extended emission is ruled out. Next, we tried to investigate point spread function, but it is difficult with the zeroth order image, since the central and adjacent pixels suffer significant pile-up. Then, we examined the first order data in spatial direction and found that 67 % of photons lie within  $\pm 1$  pixel and 87 % lie within  $\pm 2$  pixels. The encircled power radii of 50 and 80 % are 0.418 and 0.685 arcsec (0.85 and 1.4 in the unit of pixel), respectively<sup>1</sup>. Therefore, the core of the X-ray emission is not extended, and we used the response matrices for a point source in the spectral analyses.

Fig. 1 shows the lightcurve from the *Chandra* HETGS. We use *Chandra* data only from the MEG and HEG  $\pm 1$  orders. The count rate is somewhat higher during the first half of the *Chandra* observation. Simultaneously, there was a multi-wavelength campaign on this source using *ASCA*, *RXTE*, *HST*, and ground base telescopes (e.g., Turner et al. 2001 and Edelson et al. 2002). We downloaded the screened *ASCA* data from GSFC rev2 archive and created the lightcurve from June 1 to July 7. To evaluate the 2–10 keV flux state during the

---

<sup>1</sup><http://cxc.harvard.edu/cal/Hrma/hrma/misc/oac/psf2/>

*Chandra* observation, we compare the count rate and variability from *ASCA* in the *Chandra* observation with those in the whole *ASCA* observation. We summarized the average count rate and the fractional RMS variability in Table 1. During the *Chandra* observation, the source was slightly brighter than average by about 20 % and variability is typical, compared with the *ASCA* observation.

### 3. Power Spectral Density

An identifying feature of active galaxies is their X-ray variability. Their variability is not periodic but rather a featureless power law on time scales of weeks to days (e.g., Lawrence & Papadakis 1993). This is unfortunate, because no time scales that might correspond to physical size scales such as the size of the emission region, can be found.

As well as fine spectroscopy, an advantage of the *Chandra* observatory is the continuous data sampling, which allows us to compute power spectral density (PSD) directly in the frequency range around  $2 \times 10^{-4}$  Hz. In principle, because of the continuous data sampling and fairly large effective area, power spectral density analysis should allow us to observe the power spectrum on short enough time scales to look for breaks that may be indicative of a physical size scale.

We created the lightcurve binned at 64 s and calculated the power spectrum in the frequency range between  $2.0 \times 10^{-5}$  and  $7.8 \times 10^{-3}$  Hz. Fig. 2 shows the PSD of Ark 564 during the *Chandra* observation. In order to obtain reasonable signal to noise, we grouped in sets of 20 data points and averaged their logarithm (Papadakis & Lawrence 1993). The background due to Poisson noise is not subtracted and we find that it dominates the frequencies above  $10^{-2.7}(= 2.0 \times 10^{-3})$  Hz. Below this frequency, the fitted power-law index ( $\alpha$  where PSD is proportional to  $\nu^{-\alpha}$ ) is  $1.31 \pm 0.24$ . This is rather typical for AGNs on short time scales (Lawrence & Papadakis 1993).

Using the 0.7–5 keV data from the *ASCA* long-look observation, Papadakis et al. (2002) detected a high frequency break at  $(2.3 \pm 0.6) \times 10^{-3}$  Hz and a slope of  $1.24_{-0.04}^{+0.03}$  below the break frequency. Although the break frequency cannot be detected in our data due to the Poisson noise, the slope that we measure is consistent with their result.

### 4. Spectral Analyses

We analyzed the MEG $\pm$ 1 and HEG $\pm$ 1 spectra. The errors quoted in this section are 90 % for a single parameter of interest ( $\Delta\chi^2 = 2.71$ ). Calibration errors for absolute flux are

not taken into account; They are estimated to be less than 10 % and 20 % for the 1.5–6 keV band and the most of the other energy bands, respectively<sup>2</sup>. Calibration uncertainty for the relative flux between HEG and MEG is accounted for by introducing a constant parameter into the model.

#### 4.1. Continuum

First, we tried to fit the data in the whole energy band with a model consisting of a power-law and Galactic absorption ( $N_{\text{H}} = 6.4 \times 10^{20} \text{ cm}^{-2}$ ; Dickey & Lockman, 1990<sup>3</sup>). To look at the large scale behavior, we rebinned the spectra coarsely, so that the energy resolution is similar to that of the *ASCA* SIS, and so that each energy bin contains more than 25 photons. The residuals showed systematic humps with amplitude larger than the calibration errors in the softest and hardest energy bands. First we fitted the data only in the 2–5 keV band and obtained a reasonable  $\chi^2$  value of 96.1 for 110 degrees of freedom (d.o.f.). The photon-index and the unabsorbed 2–10 keV flux are  $2.56 \pm 0.06$  and  $(2.42 \pm 0.06) \times 10^{-11} \text{ erg cm}^{-2} \text{ s}^{-1}$ , respectively. Fig. 3 shows the data and the best-fit model mentioned above and extrapolated to the whole energy band. Excess emission below about 1.5 keV is seen clearly in the ratio plots.

We tried to model the soft excess component in three ways. Throughout we fixed neutral absorption to the Galactic value. First, we fitted data with a broken power-law and neutral absorption model. The fit gives a break energy of  $1.45 \pm 0.04 \text{ keV}$  and a photon-index below the break energy of  $3.11 \pm 0.03$ . The reduced  $\chi^2$  value is 1.40 for 359 d.o.f. Next we tried to fit with a two power-law model. This fit gives worse  $\chi^2_{\nu}$  value of 1.69 for the same number of d.o.f. The crossing point of the two power-laws is 1.39 keV. Finally we fitted the soft excess component with a black body model. The fit gives the blackbody temperature of  $0.124 \pm 0.003 \text{ keV}$  in the source rest frame and a better  $\chi^2_{\nu}$  value of 1.34 with the same number of d.o.f. The fits are still not acceptable. This could be due in part to the edge-like feature around 0.7 keV that can be seen in Fig. 3.

---

<sup>2</sup>e.g., <http://space.mit.edu/CXC/calib/hetgcal.html>

<sup>3</sup><http://heasarc.gsfc.nasa.gov/cgi-bin/Tools/w3nh/w3nh.pl>

## 4.2. Iron K-emission Line

Although statistically limited, HETGS data is useful to investigate narrow iron K-emission lines. We created HEG  $\pm 1$  and MEG  $\pm 1$  spectra binned at the detector resolution (FWHM). The spectra have 2–13 photons per energy bin around the iron K-energy band. Since the data are in the Poisson regime, we performed the spectral fitting and error analysis using the  $C$  statistic. We fitted the data in the 6.0–7.0 keV energy band with a power-law plus three Gaussian lines assuming all the lines are narrow and at the systemic velocity. Due to poor statistics, we performed fits fixing the power-law index at several values. With the photon-index of 2.56 (the best-fit value from the 2–5 keV band fit in §4.1), the fit gives upper-limits of the EWs of 45 eV, 53 eV and 78 eV for the neutral, He-like and H-like lines, respectively. The upper-limits are weakly subject to the assumed continuum slope, but the difference is as small as 5 eV even in a wide range of photon-index of 2.0–3.0. Thus, we can conclude that no strong narrow iron K-emission lines are detected; hence, the diskline feature with huge EW ( $653 \pm 85$  eV for Ly $\alpha$ ) reported by Turner et al. (2001) is not significantly contaminated by narrow lines.

## 4.3. Fine Spectral Features in the Soft X-ray Region

We investigated narrow features in the soft X-ray region using the HETGS high resolution spectra. We binned the HETGS first order spectra according to the following criteria: the energy bin widths are at least as large as the detector energy resolution, and each energy bin contains at least 25 photons. The latter criterion allows us to use  $\chi^2$  fitting.

First we looked at the edge-like feature around 0.7 keV. If we add an edge to the model, the fit is improved significantly (99.9% by F-test). The edge energy is  $0.711^{+0.004}_{-0.002}$  keV in the source rest frame and the optical depth is  $0.12^{+0.05}_{-0.04}$ . This energy is close to that of O VII K-edge (0.739 keV) but is inconsistent at the significance level of more than 99.9%.

Next we searched for narrow features. We estimate the continuum level by fitting the spectra with a power-law and Galactic absorption model locally in each 0.15 keV band. Fig. 5 shows the ratio of the MEG $\pm 1$  data to the continuum model. Most of narrow absorption features (O VIII Ly $\alpha$ , O VII  $1s^2-1s3p$ , Fe XVII, Ne IX  $1s^2-1s3p$  and Mg XI  $1s^2-1s2p$ ) are detected at the energies consistent with the lines at the systemic redshift. Some absorption lines of O VIII Ly $\beta$ , Ne IX  $1s^2-1s2p$ , Ne X Ly $\alpha$  are observed at slightly higher energies, suggesting blue-shift velocity is about 200 km s $^{-1}$ . However, taking into account both statistical error

and HETGS capability<sup>4</sup>, this velocity-shift is rather marginal. All the lines are unresolved (FWHM below  $\sim 400$  km s<sup>-1</sup>). The EWs are summarized in Table 2. The errors of the EWs are calculated by scaling the line normalization. Since these ions can make more absorption lines via other transitions, we searched for all lines from these ions from the transition of  $\alpha$ ,  $\beta$  and  $\gamma$  by fitting with additional absorption lines fixed at the expected energies. The results are also listed in Table 2.

There is a possibility that the line we identify as Ne x Ly $\alpha$  is seriously contaminated by an Fe xvii line. The strongest predicted line of Fe xvii is at 0.826 eV and it is marginally detected with EW of  $0.7 \pm 0.4$  eV. Another strong line feature from Fe xvii at 0.726 eV is marginally seen in Fig 5. These suggest that Fe xvii exists along our line of sight. We estimated the contribution to the Ne x Ly $\alpha$  line to have EW of  $\sim 0.5 (< 1)$  eV by scaling the EW of another Fe xvii absorption line at 1.011 keV that should be slightly weaker according to the transition probability<sup>5</sup> than the one blended with Ne x Ly $\alpha$ .

#### 4.4. Edge-like Feature at 0.712 keV

Edge-like features near 0.71 keV are frequently identified as absorption associated with the OVII K-shell. The hypothesis that we observe extremely redshifted O VII K-edge with a velocity of  $10^4$  km s<sup>-1</sup> can be ruled out, because the detected O VII absorption lines have no measurable velocity redshift (less than  $122$  km s<sup>-1</sup>). Another possibility is that the feature is composed of a combination of absorption lines from the O VII Lyman transition, an O VII K-edge and neutral iron L-edges as in the Seyfert 1 galaxy MCG–6-30-15 (Lee et al. 2001). Their data show quite strong features from both the O VII K-edge and K- $\gamma$ ,  $\delta$  lines. However, in our case, the O VII K- $\gamma$  line is not detected and its EW upper limit of 0.32 eV is one half of the best fit EW of O VII K- $\beta$ . Thus the column density of O VII is inferred not to be high enough to produce significant lines of  $\delta$  and higher. Consistently, the  $\tau_{\text{OVII}}$  of  $\sim 0.1$  in Ark 564 is much smaller than the  $\tau_{\text{OVII}}$  of  $\sim 0.7$  in MCG–6-30-15. Thus, both the redshifted edge and the Lyman transition of the O VII are unlikely to play a major role in this feature in Ark 564.

There is an alternative interpretation for the edge-like feature at 0.71 keV: it is not an edge but rather the blue cut-off of the O VIII diskline emission (Branduardi-Raymont et al. 2001). It should be noted that the iron K-emission diskline of Ark 564 observed by

---

<sup>4</sup>According to The Chandra Proposers’ Observatory Guide, systematic wavelength errors are at the  $100$  km s<sup>-1</sup> level.

<sup>5</sup>NIST atomic spectra database; [http://physics.nist.gov/cgi-bin/AtData/main\\_asd](http://physics.nist.gov/cgi-bin/AtData/main_asd)

*ASCA* (Turner et al. 2001) was predominantly from H-like iron. So, if this is the case, the innermost part of the disk should consist of two phases with quite high and moderate ionization parameter. This model is difficult to investigate only with our *Chandra* data and should be examined further using *XMM-Newton* RGS spectra.

With *XMM-Newton* and *Chandra*, deep troughs are found in the soft X-ray spectra of several Seyfert galaxies. They are inferred to be a number of iron L-absorption lines, the so-called Unresolved Transition Array (UTA) (e.g., Sako et al. 2001). If we parameterize the edge-like feature with a broad Gaussian, the fit gives central energy ( $E_c$ ), velocity width ( $\sigma$ ), and EW of  $0.738_{-0.08}^{+0.06}$  keV, 11 eV, and 4 eV, respectively. If we add the O VII K-edge at the energy fixed at the systemic velocity, the fit gives  $\tau_{\text{OVII}}$  of  $0.07_{-0.05}^{+0.04}$  and the absorption line parameters of  $E_c = 0.730 \pm 0.06$  keV ( $16.98 \pm 0.14 \text{ \AA}$ ),  $\sigma = 11 \pm 4$  eV, and EW =  $4 \pm 2$  eV (93 mÅ). Since we detected the O VII absorption lines, the latter model is more realistic. The central energy and the EW suggest that the major population of iron is Fe VII and that the column density of iron is  $\sim 3 \times 10^{16} \text{ cm}^{-2}$  (Behar, Sako, & Kahn 2001). The presence of Fe V-VI is also suggested from a significant absorption line at the energy of 0.721 keV (17.20 Å). The Fe IX ion, if the ionic fraction of it is similar to that of Fe V-VI, should make detectable lines at 16.510 Å (0.7510 keV) and 16.775 Å (0.7391 keV), and we do not detect them. Thus, we infer the ionization parameter  $\xi$ <sup>6</sup> of this absorber to be  $\sim 1$ . Assuming cosmic abundances, the column densities are estimated to be  $N_{\text{H}} \sim 10^{21} \text{ cm}^{-2}$ . This photoionization model is roughly consistent with the “lukewarm absorber” (dimensionless ionization parameter  $U$ <sup>7</sup> = 0.032 and  $N_{\text{H}} = 1.62 \times 10^{21} \text{ cm}^{-2}$ ) inferred from the absorption system in the UV band (Crenshaw et al. 2002). Their prediction of  $N_{\text{OVII}} = 1.5 \times 10^{17} \text{ cm}^{-2}$  is also consistent with the observed  $\tau_{\text{OVII}}$ , which is equivalent to  $N_{\text{OVII}} \sim 2.5_{-1.9}^{+1.8} \times 10^{17} \text{ cm}^{-2}$ . Hence, we conclude that this feature is due to a warm absorber of  $\xi \sim 1$  and  $N_{\text{H}} \sim 10^{21} \text{ cm}^{-2}$ .

---

<sup>6</sup> $\xi$  is defined as  $L/nr^2$  [erg cm s<sup>-1</sup>], where  $L$  is the hydrogen ionizing luminosity,  $n$  is the density, and  $r$  is the separation between the absorber and the source of ionization radiation.

<sup>7</sup> $U$  is defined as  $\frac{Q}{4\pi r^2 n c}$  where  $Q$  is the total number of hydrogen ionizing photons per second and  $c$  is the speed of light. For the Ark 564 spectrum,  $U$  is smaller by about 2 orders of magnitude than  $\xi$ .



## 5. Discussion

### 5.1. Physical Condition of the Higher- $\xi$ Warm Absorber

The low- $\xi$  warm absorber discussed in the previous section could be responsible for the narrow absorption lines of O VII; however, it is difficult to produce the other higher ionization lines from O VIII, Ne IX, Ne X, and Mg XI that we see. This is because, if the line-of-sight material is a single homogeneous gas, there should be some observable lines from Ne VI-VII and Mg VI-VII that are not seen. Therefore we infer that a second absorber with higher ionization is present. The suggested detection of the Fe V-VII and Fe XVII lines and the lack of the Fe IX lines also support the multi-phase/zone view.

An order of magnitude estimation of the column density ( $N_{\text{ion}}$ ) and the velocity dispersion ( $\sigma_{\text{ion}}$ ) of the ion for the higher- $\xi$  warm absorber can be made using curve of growth analysis. The detection of a pair of absorption lines from the same ion enables us to constrain  $\sigma$  and  $N$ , because the equivalent width  $EW$  of an absorption line is a function of  $N$ ,  $\sigma$ , and the oscillator strength (Spitzer 1978; Kotani et al. 2000). It should be noted that the EWs of the  $K\beta$  lines are as large as the  $K\alpha$  lines for O VIII and Ne IX ions. To explain the high value of the  $EW_{K\alpha}/EW_{K\beta}$ , at least the  $K\alpha$  lines of these ions must be saturated. This gives the upper and lower limits on  $\sigma$  and  $N$ , respectively. The  $K\delta$  lines are not useful due to poor statistics. The inferred column densities are  $N_{\text{OVII}} \sim 10^{17} \text{ cm}^{-2}$ ,  $N_{\text{OVIII}} \sim 10^{18} \text{ cm}^{-2}$ ,  $N_{\text{NeIX}} \sim 10^{17} \text{ cm}^{-2}$ ,  $N_{\text{NeX}} \sim 10^{17} \text{ cm}^{-2}$ , and  $N_{\text{MgXI}} \sim 10^{16.5} \text{ cm}^{-2}$ . The velocity dispersion is  $\sigma \sim 100 \text{ km s}^{-1}$ . Using these column densities and assuming cosmic abundances, we infer that the photoionized gas has the ionization parameter  $\log \xi \sim 2$  and the column density  $N_{\text{H}} \sim 10^{21} \text{ cm}^{-2}$ .

### 5.2. The Location of the Warm Absorbers in Ark 564

The column density and ionization parameter of the low- $\xi$  warm absorber seems to be consistent with that inferred from the high resolution UV data (Crenshaw et al. 2002). Therefore, it is plausible that the low- $\xi$  X-ray warm absorber occurs in the same gas that is responsible for the UV absorption.

Crenshaw et al. (2002) note that the high resolution *HST* STIS spectrum is unresolved in the spatial direction in both the continuum and the emission lines, and 85% of the  $\text{Ly}\alpha$  flux comes from a region smaller than  $0''.2$ . From this they infer that the narrow-line region in this object is more compact than 95 pc. Narrow-line region (NLR) sizes of  $\sim 100 \text{ pc}$  appear to be rather typical in Seyfert 1 galaxies (Schmitt & Kinney 1996). Because the  $\text{Ly}\alpha$  and C IV

absorption lines are saturated, and are not filled in by emission from the NLR, Crenshaw et al. infer that the absorber must fully cover the narrow-line region. They also note that the inferred ionization parameter and density for the warm absorber are such that the warm absorbing gas should emit optical lines. They are forced to conclude that the global covering factor for the warm absorber is 0.05 or less so that the strength of the predicted optical emission lines are consistent with that observed. They infer that for a distance to the warm absorber of more than 95 pc, the density should be  $\leq 10^3 \text{ cm}^{-3}$ .

We note that if the NLR is as large as 95 pc, and the warm absorber is present only toward our line of sight (i.e., the absorption is not axisymmetric), the distance to the absorber may be as small as 95 pc and still present a global covering fraction of only 0.05. We note that despite the fact that UV absorption occurring along with X-ray absorption is found in about 50% of active galaxies (Crenshaw et al. 1999), an absorber presenting a covering factor of 0.05 in a random direction cannot be commonly seen in active galaxies, simply because the small covering fraction means that the probability of finding the warm absorber between the viewer and the nucleus is low.

The likelihood of seeing such absorption may be increased if the absorber is associated with a component that we know is already present in AGN. Therefore, we suggest the possibility that the warm absorber for Ark 564 may occur within the narrow-line region itself. The absorption troughs may not be filled in by  $\text{Ly}\alpha$  and C IV produced in the narrow-line region if those lines are not strong in Ark 564. As discussed by Crenshaw et al. Ark 564 is heavily reddened. If the dust responsible for the reddening is located in the narrow-line region, that dust can reduce the resonance line emission by absorption (e.g., Voit, Weymann & Korista 1993; Hamann, Korista, & Morris 1993; Ferguson et al. 1997). Other evidence discussed by Netzer & Laor (1993) points to the presence of dust in the NLR. The ionization parameter and density inferred for the absorber by Crenshaw et al. are not terribly different than those inferred for the narrow-line region (e.g., Kraemer et al. 1994).

The high- $\xi$  warm absorber may be coincident with the low- $\xi$  warm absorber. If so, a lower density by 2 orders of magnitude would be inferred. Circumstantial evidence for this scenario is the fact the velocity offsets of the UV and X-ray absorbers are consistent with one another, as far as we can tell. It should be noted that the outflow velocity of 106–197  $\text{km s}^{-1}$  revealed by the *HST* STIS echelle (Crenshaw et al. 2002) is difficult to be detected by the HETGS because of the relatively poorer data quality of *Chandra* compared with *HST*.

However, it is not necessary for the high- $\xi$  warm absorber to be coincident with the low- $\xi$  one. Close examination of the regions of the spectrum right around the absorption lines reveals suggestions of emission line wings tailing toward higher and lower energies (e.g., the higher and lower energy side of the O VIII  $\text{Ly}\alpha$  and Ne X  $\text{Ly}\alpha$  lines, respectively), although

most of these features are not statistically significant. These structures resemble those in the UV in which the center of the emission lines has been removed by the nearly saturated broad absorption lines such that only the high and low energy wings of the line remains (Crenshaw et al. 2002). The warm absorber shows us ionized gas along our line of sight and the same photoionization may also power emission lines in the gas predominately out of our line to the central source if the covering fraction is large enough.

### 5.3. Comparison of the Warm Absorbers with those in other NLS1s

*Chandra* grating observations have been reported from three NLS1s. In NGC 4051, Collinge et al. (2001) found many absorption lines from highly ionized ions such as oxygen, neon, silicon and sulphur. They resolved two distinct absorption systems with high outflow velocity ( $2340 \pm 130 \text{ km s}^{-1}$ ) and low outflow velocity ( $600 \pm 130 \text{ km s}^{-1}$ ). On the other hand, no absorption lines were detected in the spectrum of Ton S180 (Turner et al. 2001) and Mrk 478 (Marshall et al. 2003). The properties of the absorber in Ark 564 are different from both of them.

Although it is properly classified as a Seyfert 1 galaxy and has relatively narrow optical lines, the features reported from MCG–6-30-15 by Lee et al. (2001) are similar to what we found in Ark 564. Specifically, they also detected narrow absorption lines from He-like and H-like oxygen without detectable velocity shifts. Moreover, in the O VII K-edge range, the deficit starts at an energy lower by about 30 eV than the energy of O VII K-edge. Absorption lines possibly from ionized iron are also detected. All of these features are common between MCG–6-30-15 and Ark 564.

To date, results from the *XMM-Newton* RGS observations of NLS1s are reported on Mrk 766 and Mrk 359. Absorption features from O V–VIII are detected in Mrk 766 and is very similar to that of MCG–6-30-15 (Branduardi-Raymont et al. 2001; Sako et al. 2003). On the other hand, Mrk 359 does not show absorption lines but rather emission lines from O VII and Ne IX (O’Brien et al. 2001).

It is still difficult to have unified view of warm absorber residing in NLS1s. There are two objects lacking the detection of warm absorber: Ton S180 is the most luminous among the six objects, whereas the other of Mrk 359 is less luminous than the Ark 564 and Mrk 766 with warm absorber. Even though luminosity could be considered to be one of the primary parameters to make variety of warm absorber, we cannot simply explain this difference only by the difference in luminosity. Regarding the outflow, to launch it by radiation in the gravity from a central black hole, higher luminosity normalized by Eddington ( $L/L_E$ ) is

required (Reynolds & Fabian 1995). However, NGC 4051 with the fastest outflow has the lowest  $L/L_E$ , if we estimate the central mass from the reverberation mapping technique (Kaspi et al. 2000). Again, the outflow velocity seems difficult to be explained simply by one parameter of  $L/L_E$ .

We also examined optical spectra from Ton S180 and NGC 4051 (kindly supplied by Jules Halpern), Ark 564 (from HST archive), and Mrk 478 and Mrk 766, and MCG–6-30-15. We looked for differences in the [O III] lines from the narrow-line region, the broad component of  $H\beta$ , as well as He II and coronal lines which have been suggested to be associated with the warm absorber (Peterson et al. 2000; Porquet et al. 1999). The clearest difference that we found was that Ton S180 and Mrk 478 lacked coronal line emission (Here we looked at the Fe X and Fe VII lines), while all of the other objects had coronal lines. Furthermore, Ton S180 and Mrk 478 had blueward-asymmetric [O III] lines, while the other objects had rather symmetric [O III] lines. Since Ton S180 and Mrk 478 seem unusual in our comparison for its lack of X-ray absorption lines and low equivalent width FUV absorption lines, this result perhaps supports the idea that the warm absorber is associated with coronal line emission.

#### 5.4. The 1 keV Emission Line-like Feature

The *Chandra* observation allowed us to advance our understanding of the spectrum of Ark 564. We found no prominent narrow emission line around 1 keV and ruled out the possibility that the 1 keV feature originates from blends of several narrow emission lines. However, the possibility remains that a broad emission line could be present that is not easily seen in the somewhat low-signal-to-noise spectrum.

To investigate a broad emission line, we fitted the MEG and HEG first order spectra binned at *ASCA* resolution with a model consisting of a power-law, blackbody and a Gaussian line near 1 keV. The line width  $\sigma$  was fixed at 100 eV. The fit gives a center energy of  $1.02 \pm 0.03$  keV and the EW of  $18 \pm 7$  eV. The energy is consistent with the results from *ASCA* but the EW is smaller.

Although the detected absorption lines with the EWs of  $\sim 1$  eV cannot be seen in spectra with medium energy resolution, the predicted absorption edges may be apparent. We speculate that the 1 keV feature is an artifact of the edges. In order to investigate this point, we add both the inferred UTA and the edges from the low and high- $\xi$  warm absorbers, fixing the parameters to be best-fit values, to the model. The spectral model *absori* in *XSPEC* was used for the model of the edges of warm absorbers. Then, the center

energy of the broad line becomes  $1.02_{-0.04}^{+0.05}$  keV and the EW becomes  $9 \pm 7$  eV. Although the decrease of the EW is not statistically significant, the EW is smaller and nearly consistent with zero. Furthermore, the fit with the two warm absorbers was not significantly improved by adding the broad line component to the model (85 % significance by F-test). Thus the 1 keV feature appears to be consistent with being an artifact of the warm absorber, although we cannot completely rule out a broad emission line or blends of many narrow absorption lines.

## 6. Summary

From our *Chandra* HETGS observation, we confirmed the presence of the soft excess. If we fitted the excess with blackbody model, the best-fit temperature is 0.124 keV. No prominent narrow emission lines are observed around 1 keV. We detected an edge-like feature at 0.712 keV in the source rest frame. The preferred interpretation of this feature is combination of the O VII K-edge and a number of the L-absorption lines from the slightly ionized iron, which suggests a warm absorber with  $\xi \sim 1$  and  $N_{\text{H}} \sim 10^{21}$  cm $^{-2}$ . These properties are roughly consistent with those of the UV absorber. We also detected narrow absorption lines of O VII, O VIII, Ne IX, Ne X, and Mg XI at the systemic velocity. From these lines, another warm absorber having  $\log \xi \sim 2$  and  $N_{\text{H}} \sim 10^{21}$  cm $^{-2}$  is required.

We acknowledge the great efforts of all the members of the *Chandra* team. We are grateful to Prof. Jules Halpern for reduction of optical spectra and helpful discussion. We thank John Moore for his analyses of optical spectra. We also thank an anonymous referee for careful reading and helpful comments. CM and KML gratefully acknowledge support through the *Chandra* GO 0-11624 grant. HLM is supported by SAO contract SV1-61010 to MIT.

## REFERENCES

- Behar, E., Sako, M., & Kahn, S. M. 2001, ApJ, 563, 497
- Brandt, W. N., Fabian, A. C., Nandra, K., Reynolds, C. S., & Brinkmann, W. 1994, MNRAS, 271, 958
- Branduardi-Raymont, G., Sako, M., Kahn, S. M., Brinkman, A. C., Kaastra, J. S., & Page, M. J. 2001, A&A, 365, L140

- Clements, E. D. 1981, MNRAS, 197, 829
- Collinge, M. J., et al. 2001, ApJ, 557, 2
- Comastri, A., et al. 2001, A&A, 365, 400
- Crenshaw, D. M., Kraemer, S. B., Boggess, A., Maran, S. P., Mushotzky, R. F., & Wu, C.-C. 1999, ApJ, 516, 750
- Crenshaw, D. M., et al. 2002, ApJ, 566, 187
- Dickey, J. M., Lockman, F. J. 1990, ARA&A, 28, 215
- Edelson, R., Turner, T.J., Vaughan, S., Markowitz, A., Marshall, H. Dobbie, P. & Warwick, R. 2002, ApJ, 568, 610
- Ferguson, J. W., Korista, K. T., Baldwin, J. A., & Ferland, G. J. 1997, ApJ, 487, 122
- Goodrich, R. W. 1989, ApJ, 342, 224
- Hamann, F., Korista, K. T., & Morris, S. L. 1993, ApJ, 415, 541
- Huchra, J. P., Vogeley, M. S., & Geller, M. J. 1999, ApJS, 121, 287
- Kaspi, S., Smith, P. S., Netzer, H., Maoz, D., Jannuzi, B. T., Giveon, U. 2000, ApJ, 533, 631
- Kotani, T., Ebisawa, K., Dotani, T., Inoue, H., Nagase, F., Tanaka, Y., Ueda, Y. 2000, ApJ, 539, 413
- Kraemer, S. B., Wu, C.-C., Crenshaw, D. M., & Harrington, J. P. 1994, ApJ, 435, 171
- Laor, A. 2000, NewA Rev., 44, 503
- Lawrence, A., & Papadakis, I. E. 1993, ApJ, 414, L85
- Lee, J. C., et al. 2001, ApJ, 554, L13
- Leighly, K. M. 1999a, ApJS, 125, 297
- Leighly, K. M. 1999b, ApJS, 125, 317
- Marshall, H. L., Edelson, R. A., Vaughan, S., Malkan, M., O'Brien, P., Warwick, R. 2003, AJ, 125, 459
- Netzer, H., & Laor, A. 1993, ApJ, 404, L51

- O’Brien, P. T., Page, K., Reeves, J. N., Pounds, K., Turner, M. J. L., & Puchnarewicz, E. M. 2001, MNRAS, 327, L37
- Osterbrock, D. E., & Pogge, R. W. 1985, ApJ, 297, 166
- Papadakis, I. E., & Lawrence, A. 1993, MNRAS, 261, 612
- Papadakis, I. E., Brinkmann, W., Negro, H., & Gliozzi, M. 2002, A&A, 382, L1
- Peterson, B. M., et al. 2000, ApJ, 542, 161
- Porquet, D., Dumont, A.-M., Collin, S., & Mouchet, M. 1999, A&A, 341, 58
- Reynolds, C. S. & Fabian, A. C. 1995, MNRAS, 273, 1167
- Sako, M., et al. 2001, A&A, 365, L168
- Sako, M., et al. 2003, ApJ, 596, 114
- Schmitt, H. R., Kinney, A. L. 1996 ApJ, 463, 498
- Spitzer, L., Jr. 1978, “Physical Processes in the Interstellar Medium”
- Turner, J. T., George, I. M., & Netzer, H. 1999, ApJ, 526, 52
- Turner, J. T., Romano, P., George, I. M., Edelson, R., Collier, S. J., Mathur, S., & Peterson, B. M. 2001, ApJ, 561, 131
- Voit, G. M., Weymann, R. J., & Korista, K. T. 1993, ApJ, 413, 95

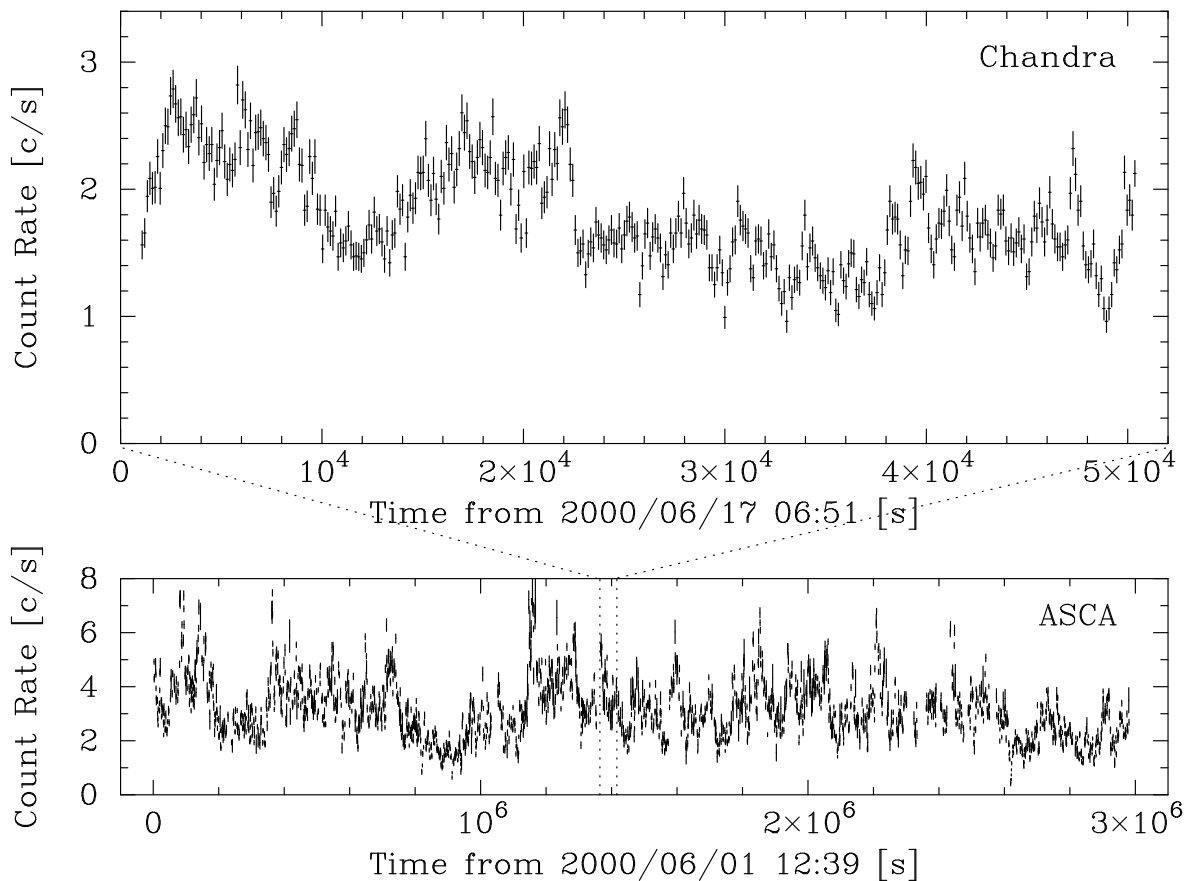


Fig. 1.— Upper: The lightcurve from the *Chandra* HETGS binned at 128 s. The positive and negative first order data from both the HEG and the MEG are combined. Lower: The lightcurve from the *ASCA* SIS detectors. The period of our *Chandra* observation is marked by dotted lines. The energy range of HETGS and SIS are 0.4–10 and 0.5–10 keV, respectively.



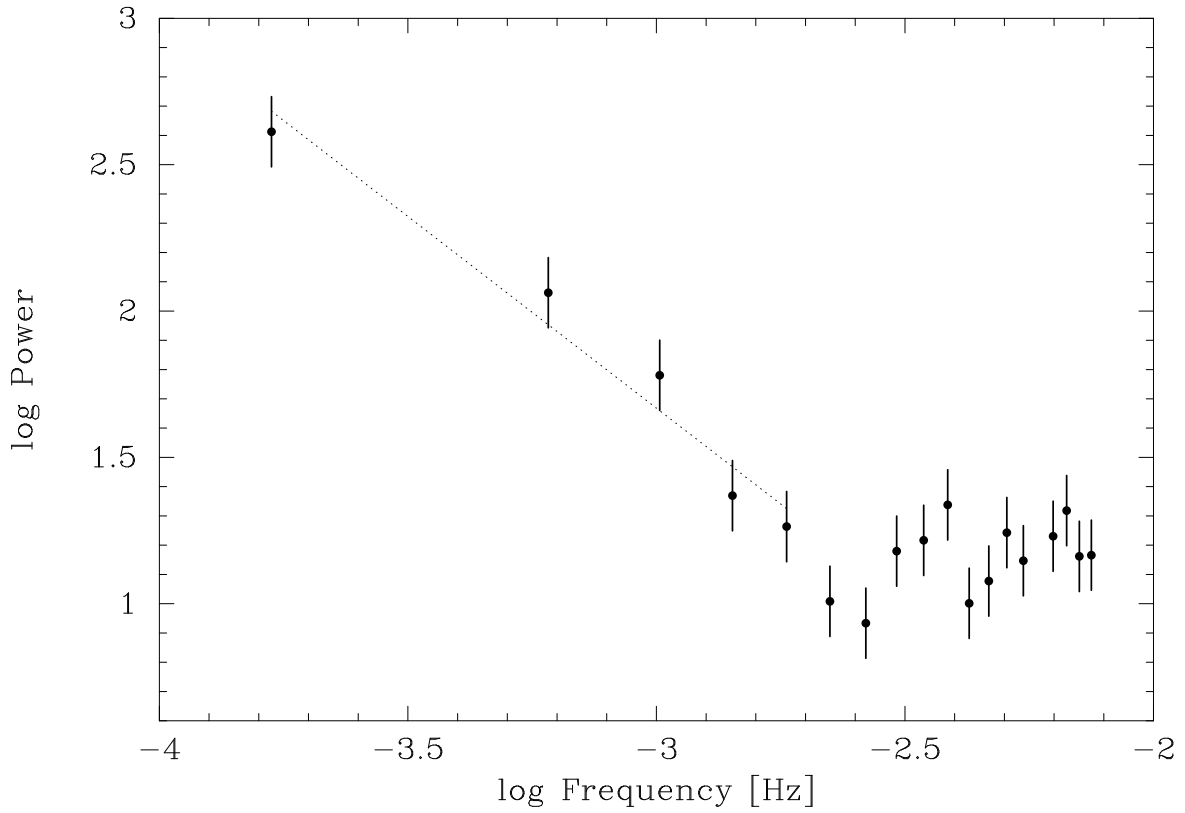


Fig. 2.— Power density spectrum of Ark 564 during the *Chandra* observation. We grouped the data and calculated the errors in the manner described in Papadakis & Lawrence (1993). The dotted line shows the best-fit power-law model in the frequency range of  $1.7 \times 10^{-4}$  to  $2.0 \times 10^{-3}$  Hz. The power-law index is  $1.31 \pm 0.24$ .

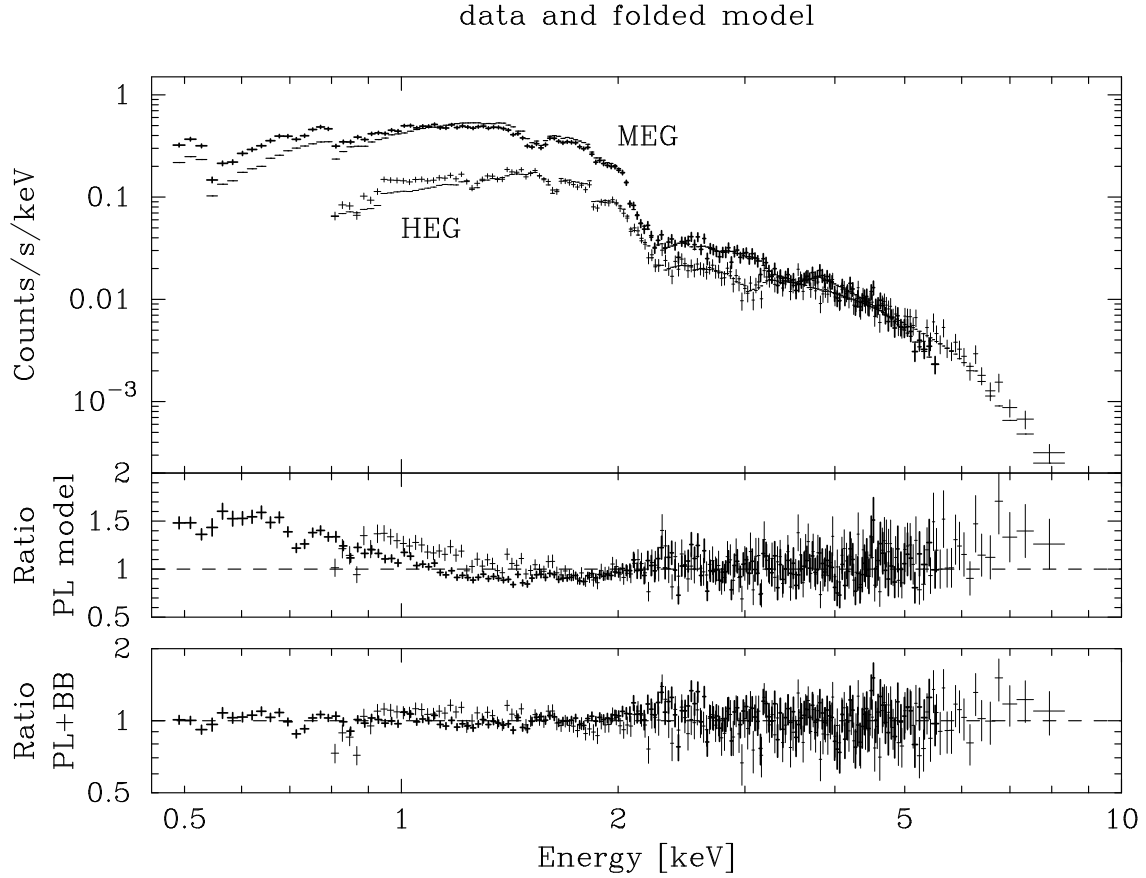


Fig. 3.— Top: The HETGS spectra and the best-fit power-law model in the 2–5 keV band. The MEG $\pm$ 1 and HEG $\pm$ 1 are thick and thin lines, respectively. Middle: The ratios of data to the power-law model extrapolated to the whole energy band. Bottom: The ratios to the power-law plus black body model. All models include Galactic absorption.

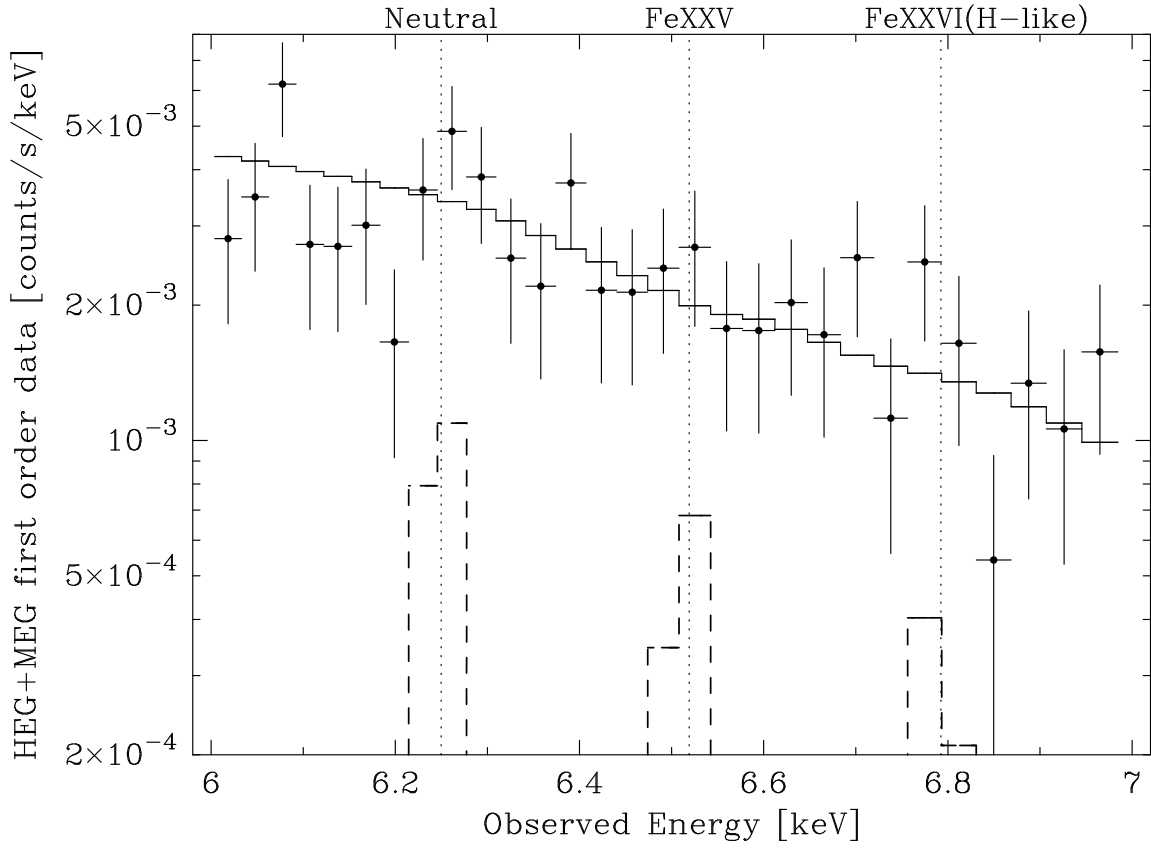


Fig. 4.— The HETGS spectrum in the iron K-line energy band. The HEG±1 and MEG±1 are added for plot. The solid stepped line shows power-law continuum level. The energies of neutral, He-like and H-like iron K-line are marked with the dotted lines. For reference, the lines with the EW of 20 eV are shown by the dashed line.

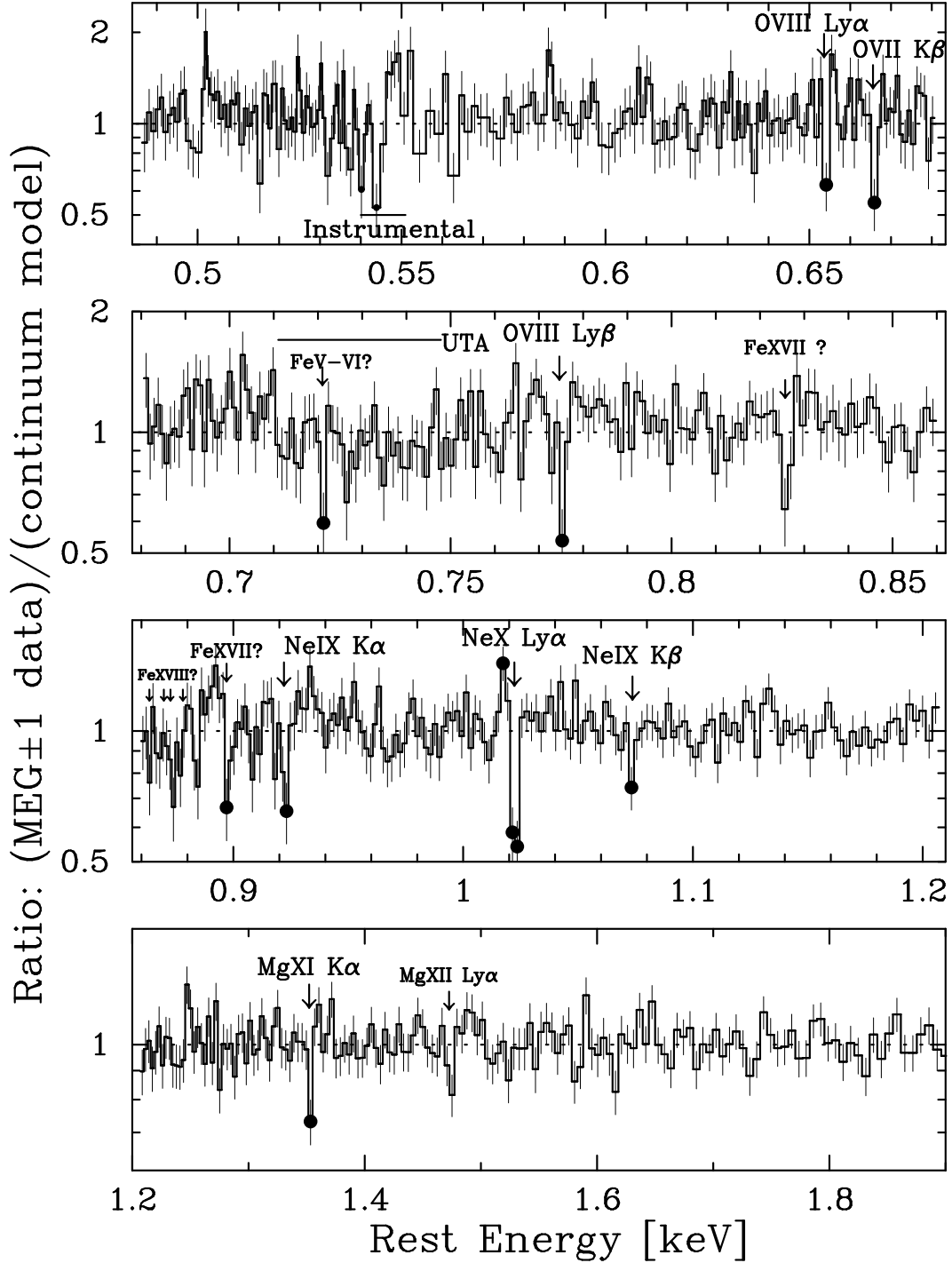


Fig. 5.— The ratio of MEG±1 data to a continuum model. Features detected at significance level of more than  $3.0\sigma$  are marked by  $\bullet$ . A broad deficit also can be seen between 0.71–0.75 keV. The labels with “?” denote suggested IDs.

Table 1. The 2–10 keV flux state during the *Chandra* and *ASCA* observations. The *Chandra* data are from the MEG and HEG  $\pm 1$  orders. The background is negligible in HETGS. The *ASCA* data are from the GISs. The background is subtracted.

Observation	Count Rate [c/s]	RMS <sup>a</sup>
<i>Chandra</i>	$0.259 \pm 0.002$	$24.6 \pm 1.6$
<i>ASCA</i> simultaneous with <i>Chandra</i>	$0.659 \pm 0.007$	$24.8 \pm 2.0$
<i>ASCA</i> whole (6/1–7/6)	$0.546 \pm 0.001$	$25.1^b$

<sup>a</sup>The time bin width is 256 s.

<sup>b</sup>The RMS was calculated in every interval with the same span as the *Chandra* observation, then their average is calculated.

Table 2. Parameters of narrow absorption lines from the Gaussian fit. All lines are unresolved.

$E_{obs.}^a$ [eV]	$E_{lab}^b$ [eV]	EW [eV]	Identification ion & transition	EWs of possible accompanying lines from the ion <sup>c</sup>		
				$\alpha$	$\beta$	$\gamma$
$654.0^{+0.7}_{-1.3}$	653.5	$0.68^{+0.36}_{-0.32}$	O VIII Ly $\alpha$	—	$0.71 \pm 0.33$	$-0.33 (< 0.40)^f$
$666.2^{+0.4}_{-0.9}$	665.6	$0.74^{+0.41}_{-0.29}$	O VII $1s^2-1s3p$	$0.19 (< 0.69)$	—	$-0.06 (< 0.32)$
$721.1^{+0.6}_{-0.5}$	(719–722)	$0.57^{+0.29}_{-0.29}^e$	(Fe V–VI)	—	—	—
$775.4^{+0.4}_{-0.6}^d$	774.6	$0.69^{+0.25}_{-0.26}$	O VIII Ly $\beta$	$0.75 \pm 0.40$	—	$-0.33 (< 0.40)^g$
$897.5^{+0.5}_{-1.0}$	(896.8)	$0.59^{+0.32}_{-0.32}^f$	(Fe XVII)	—	—	—
$922.6^{+0.7}_{-0.4}^d$	922.0	$0.92^{+0.37}_{-0.43}$	Ne IX $1s^2-1s2p$	—	$0.76 \pm 0.38$	$0.26 (< 0.76)$
$1022.5^{+0.3}_{-0.5}^d$	1021.9	$1.84^{+0.42}_{-0.38}$	Ne X Ly $\alpha$ (+ Fe XVII)	—	$0.13 (< 0.62)$	$0.49 (< 1.09)$
$1073.8^{+0.6}_{-1.4}$	1073.7	$0.76^{+0.57}_{-0.40}$	Ne IX $1s^2-1s3p$	$0.79 \pm 0.42$	—	$0.26 (< 0.76)$
$1353^{+1}_{-1}$	1352.2	$1.15^{+0.58}_{-0.50}$	Mg XI $1s^2-1s2p$	—	$0.48 (< 1.29)$	$0.43 (< 1.21)$

<sup>a</sup>The best-fit value of the line central energies in the source rest frame.

<sup>b</sup>The theoretical line energies from references

<sup>c</sup>The EWs are derived from the Gaussian fits at fixed energies with fixed velocity width of 0, which result in slightly different values from the EWs in the third column from the Gaussian fits with free center energy and free velocity width.

<sup>d</sup>The 90 % lower limit is slightly larger than  $E_{lab}$  by 0.1–0.2 eV (corresponding velocity of several ten km s<sup>-1</sup>).

<sup>e</sup> The EW is subject to the continuum modeling because it is part of a broad deficit. The velocity width of  $\sigma$  is fixed at 0.

<sup>f</sup>The central energy is fixed at the best-fit value during the EW error estimation.  $\sigma = 0$  is assumed.

<sup>g</sup>Only the MEG+1 data are used, because this feature in the MEG–1 data falls in the chip gap.